# Ionospheric density oscillations associated with recurrent prompt penetration electric fields during the space weather event of 04 November 2021 over the East-Asian sector

Ram Singh[1], Y.S Lee[1], S.M. Song[1], Y.H. Kim[1], Jong Yeon Yun[2], S. Sripathi[3], B. Rajesh[3]

[1]Department of Astronomy and Space Science, Chungnam National University, Daejeon, South Korea

[2]Forecast &Observation Division, Korea Space Weather Center (KSWC), Jeju, South Korea

[3]Indian Institute of Geomagnetism (IIG), Mumbai, India

Corresponding author: Young-Sook Lee (yslee0923@cnu.ac.kr)

**Abstract:**

We found the signatures of the multiple prompt penetration electric fields (PPEF) and the disturbance dynamo (DD) electric field having impacts on the East Asian sector ionosphere along the meridional chain thoroughly from the equator, low-mid to high latitudes during the space weather event of 03-05 November 2021. The observation is made on GPS-TEC, digisonde, and magnetometer stations. In the main phase of the storm, intense modulations of VTEC (vertical total electron content) and foF2 (critical frequency) are observed as coherently fluctuating with IEF (interplanetary electric field) and IMF Bz reorientations. It is diagnosed that the oscillations in the DP2 (disturbance polar current 2) current system directly penetrate meridianally from high to equatorial latitudes, leading to the significant changes in ionospheric electrodynamics that governs the density fluctuations. The wavelet spectra of VTEC, foF2, h'F (virtual height), H-components and IEF give a result of common and dominant periodicity occurring at ~1hr. This result suggests that the wavelike oscillations of VTEC and foF2 and H component are associated with PP electric fields.

**Plain Language Summary:**

Geomagnetic storm time electrodynamics of the ionosphere is severely affected by magnetospheric convection electric field induced by solar wind-induced magnetospheric dynamo, and ionospheric disturbance dynamo (DD) generated by global thermospheric wind circulation and joule heating at high latitude. The Magnetospheric convection electric field can

penetrate instantly into the equatorial ionosphere known as prompt penetration (PP) electric field, while, the thermospheric wind and its associated disturbances can reach at the equator with a time delay. During the main phase of the storm, observations showed intense modulations in vertical total electron content (VTEC), critical frequency (foF2) from equator to high latitudes associated with PP electric fields. In recovery phase, disturbances in VTEC, foF2, and virtual height (h'F) are caused by either DD electric field or traveling ionospheric disturbances (TIDs). Further analysis in this study suggests the evidence of causal relationship among the interplanetary electric field, DP2 current system, and ionospheric density oscillations. Wavelets analysis shows a common and dominant periodicity of ~1 hr in interplanetary and ionospheric parameters.

**Keywords:** Ionospheric electrodynamics; high-mid-low latitude ionosphere; geomagnetic storm, GPS-TEC, prompt penetration of electric field (PPEF), digisonde

**Key Results:**

(1) PPEF signature observed along the ionosphere meridian in East-Asia.
(2) Infiltration of DP2 current to the equator to cause the ionospheric density fluctuations.
(3) The oscillations of the observed parameters (TEC, foF2 and H-component) along the meridional chain coincide with that of IEF at a ~1hr periodicity.

## 1. Introduction:

It is well known that the interplanetary and geomagnetic conditions play a significant role in the interaction between the magnetosphere and ionosphere during geomagnetic storms. The high-speed solar wind interacts with the magnetosphere and discharges its energy into the high latitude ionosphere through magnetospheric field-aligned currents (FACs) and other sources (Araki et al., 1985; Kikuchi, 1986; Kikuchi et al., 1996, 2008). This energy blows towards the equator in the form of neutral winds, electric fields, or other processes, that can modify the electrodynamics of the ionosphere (Blanc and Richmond, 1980; Kikuchi, 1986; Sastri et al., 1997; Kamide et al., 1997, 1998; Abdu et al., 1998). The modifications in the electrodynamics of the magnetosphere-ionosphere system can impact space and ground-based technological systems. The main phase of a geomagnetic storm, which is associated with ring current intensification, leads to large changes in the electrodynamics of equatorial and low latitude ionospheres, playing as a risk factor for power systems at middle and low latitudes (Gaunt and

Coetzee, 2007; Liu et al., 2009).

At the equatorial and low latitudes the ionospheric electric field and currents are mainly driven by the prompt penetration electric field (PPEF) induced by the magnetospheric convection electric field associated with the solar-wind magnetosphere dynamo (Araki et al., 1985; Kikuchi, 1986; Spiro et al., 1988; Sastri et al., 1997). Neutral wind perturbations caused by storm-induced high-latitude joule heating can change thermospheric general circulation and plasma dynamics. Ions can move either along or perpendicular to the magnetic field by the ion-neutral collision caused by the neutral wind disturbance. Parallel ion drift can generate the traveling ionospheric disturbance (TID), and perpendicular ion drift is associated with zonal electric field established by disturbance wind dynamo to be induced during the equatorward propagation of disturbance winds. Therefore, the lower latitude ionospheres are significantly affected either by the ionospheric disturbance dynamo electric field (DDEF) or TID (Fujiwara et al., 1996; Blanc and Richmond, 1980; Spiro et al., 1988; Sastri et al., 1997; Abdu, 1997; Abdu et al., 1998). For the PPEF the ionospheric convection electric field, which is projected from the magnetosphere, promptly induce DP2 current (disturbance polar current 2) system in the dusk and dawn sides at the equatorward edges in the convection zones, and then the effects of DP2 currents promptly penetrate into the low and equatorial latitudes.

The effects of PP electric field instantaneously penetrate into the equator by the propagation of eastward/westward polarity in the transverse magnetic mode (TM0) through the Earth-Ionosphere waveguide in the dayside/nightside [Kikuchi et al., 1996]. However, the DD electric field reaches at the equator with a delay depending upon its propagation speed with westward/eastward polarity on the dayside/nightside. The DD electric field disturbances are long-lasting, and their impacts on the equatorial and low-latitude ionosphere can be seen up to about a day or two after the onset of a geomagnetic storm (Blanc and Richmond, 1980; Sastri et al., 1997; Abdu et al., 1998).

The storm time ionospheric electric field perturbations affect the distribution of ionospheric plasma density by generating positive and negative ionospheric storms. It is known that the enhancement in electron density/total electron content (TEC)/maximum frequency of F2 peak (foF2) as compared to quiet time variation is considered as positive ionospheric storm, while the reduction of electron density/TEC/foF2 is termed with the negative ionospheric storm. The positive ionospheric storms can be generated by plasma redistribution due to disturbed electric fields (Reddy et al., 1990; Kelley et al., 2004; Lin et al., 2005; Balan et al., 2010; Lu et al., 2012; Ram Singh et al., 2015; Fagundes et al., 2016; Ram Singh and Sripathi, 2017), by thermospheric winds (Prolss et al., 1991; Prolss, 1993), by composition changes and an increase in the oxygen density (Rishbeth, 1991; Fuller-Rowell et al., 1996), or by traveling ionospheric disturbances (TIDs) (Goncharenko et al., 2007; Liu et al., 2014). However, the negative ionospheric storms are attributed to an increase of molecular nitrogen density relative to atomic oxygen (Prolss et al., 1988; Rishbeth, 1998). Several authors investigated positive and negative ionospheric storm effects on the topside and bottom side ionospheres using the GPS-TEC and ground based ionosondes (Zhao et al., 2012; Fagundes et al., 2016; Lima et al., 2004; Kelley et al., 2004; Ram Singh and Sripathi., 2017). Fagundes et al. (2016) reported positive ionospheric storms in F-region density distribution, which were associated with the strong eastward PPEF over the Brazilian sector during the main phase of the magnetic storm on 17 March 2015. Kelley et al. (2004) suggested that the daytime eastward PPEF can generate negative storms in Nmax (maximum electron density) and TEC at the equatorial latitudes, while positive storms at the higher latitudes may occur through the enhanced plasma by fountain effects (Balan et al., 2010). Several modeling studies also suggested that the PPEF alone can produce positive ionospheric storms (Lu et al., 2012; Joshi et al., 2016).

The turning of the interplanetary magnetic field Bz plays an important role in characterizing the dawn to dusk convection electric field ($\mathrm{Ey} = -\mathrm{Vx} \times \mathrm{Bz}$) in the magnetosphere, which penetrates into the polar ionosphere and finally generates the DP1 (disturbance polar current 1) and DP2 current systems in the high-latitude ionosphere (Nishida, 1968a, 1968b; Araki et al., 1985; Kikuchi et al., 1996). The DP1 and DP2 current systems are originated from auroral electrojets and magnetic perturbations, which are generated by substorms and the convective system in the magnetosphere, respectively. When the polarity of IMF Bz suddenly turns from north to south, the magnetospheric convection electric field is intensified DP2 current system fluctuates and extends its effects down to the equatorial latitudes until the plasmasphere is electrically shielded (Nishida, 1968a, 1968b). During the northward turning of IMF Bz, the intensity of the convection electric field is reduced and a strong electric field becomes effective in the plasmasphere that has the opposite polarity (dusk to dawn) (Kelley et al., 1979; Araki et al., 1985; Kikuchi et al., 1996; Kelley et al., 2007). The DP2 current system is directly associated with the magnetospheric convection or the turning of IMF Bz. The impact can be detected at all latitudes with different magnitudes (Clauer and Kamide, 1985). Using the spacecraft and ground magnetometer observations, many studies have suggested that the DP2 current disturbances are global, characterized by the quasi-periodic magnetic fluctuations with a timescale of 30 min to several hours (Nishida, 1968a, 1968b; Kikuchi et al., 2008, Chakrabarty et al., 2008; Yizengaw et al., 2016, Huang., 2019a, 2020).

Several studies have focused on the fluctuations of DP2 currents and their impact on magnetic fluctuations in the equatorial ionosphere (Nishida, 1968a; Wei et al., 2008; Yizengaw et al., 2016, Huang., 2019a, 2020). Nishida (1968a) reported that the DP2 currents in the high-latitude and equatorial regions coherently fluctuate with IMF Bz, and the presence of DP2 current fluctuations at the equator are the direct result of quasi-periodic oscillations of IEF (interplanetary electric field) penetrating into the magnetosphere, and reaching down to the equatorial ionosphere (Kikuchi et al., 2008). The fluctuations of DP2 current systems in the high-latitude and the equatorial ionospheres are primarily driven by the fluctuations of IMF Bz (Wei et al., 2008; Yizengaw et al., 2016; Huang., 2019a, 2020). Yizengaw et al. (2016) presented coherent fluctuations of the IMF Bz, ionospheric DP2 currents, GPS TEC at the equatorial latitudes, and equatorial electrojet (EEJ). They suggested that the DP2 current fluctuations are generated by the reorientations of IMF Bz, which penetrate into the equatorial ionosphere and produce the fluctuations in the GPS TEC and EEJ.

Although DP2 current systems and their impact on magnetic fluctuations in the equatorial ionospheric region were studied in quite a few ways (Nishida, 1968a; Clauer and Kamide, 1985; Kikuchi et al., 1996, 2008), there are still several important questions remained unsolved. The main question is whether the impact of the DP2 current system can disturb the ionospheric density distribution at all latitudes at the same time. This study investigates the response of the ionospheric density distribution to the fluctuations of the DP2 current system at the high-mid and low latitudes over the East Asian sector during an intense geomagnetic storm on 03-05 November 2021.

This article is organized in the following manner; the data sources of the analysis are presented in section 2. In section 3, observations and results are presented. The space weather conditions and ground based observations are presented in sections 3.1 and 3.2. In section 3.3, the wavelet analysis is performed to find a common periodicity of VTEC, H-component, foF2, h’F, and IEFy. Discussions and conclusions are presented in sections 4 and 5, respectively.

## 2. Data Sets:

To investigate the ionospheric response to the space weather event of 03-05 November 2021, we analyzed multi-instrument data sets over the East Asian sector. Solar wind parameters were obtained from the CDAWeb (http://cdaweb.gsfc.nasa.gov/). The 1 min time resolution solar wind data (in GSM coordinates) are measured by the ACE satellite, which is located near the L1 point. The vertical TEC (VTEC) data were obtained from a meridional chain of GPS receivers over the East Asian sector from (ftp://cddis.gsfc.nasa.gov/pub/gps/data, C. Noll, 2010), and 5 min interval GPS TEC data were collected from MIT Haystack Observatory Madrigal database (http://madrigal.haystack.mit.edu/madrigal/). The ionospheric parameters, namely, h'F (virtual height) and foF2 data were obtained from ionosondes operating at Guam (GUA: 13.69°N, 144.86°E, Geom. 6.12$^{o}$N), Sanya (SA: 18.53$^{o}$N, 109.61$^{o}$E, Geom. 8.87$^{o}$N), Wuhan (WU: 30.50$^{o}$N, 114.40$^{o}$E, Geom. 21.04$^{o}$N), Jeju (JJ: 33.43°N, 126.30°E, Geom. 24.36$^{o}$N), Icheon (ICN: 37.14°N, 127.54°E, Geom. 28.11$^{o}$N), Beijing (BP: 40.30$^{o}$N, 116.20$^{o}$E, Geom. 30.85$^{o}$N), and Mohe (MH: 52.00$^{o}$N, 122.52$^{o}$E, Geom. 42.73$^{o}$N). The ionograms at JJ, ICN, and BP are recorded in 15 min intervals, while the time interval of the ionograms at GUA, SA, WU, and MH is ~7 min. Ionosonde data were collected from Global Ionosphere Radio Observatory (GIRO) web (https://giro.uml.edu/didbase/). The geomagnetic activity indices of the symmetric component of ring current (SYM-H) and Kp index were obtained from the WDC (http://wdc.kugi.kyoto-u.ac.jp/). Magnetic field data were taken from the SuperMAG magnetometer network (http://supermag.jhuapl.edu) and the Korean space weather center (https://spaceweather.rra.go.kr). Details of the GPS TEC stations, ionosondes, and magnetometers with name, station code, latitudes, and longitudes are listed in Table 1, and the location of stations used in the present study are shown in Figure 1.

## 3. Observational Results

### 3.1 Space weather conditions during the storm of 03-05 November 2021

In this study, we report the unique observation of the quasi-periodic oscillations of the electron density at the high-mid and low latitude ionosphere over the East Asian sector caused by the PP electric field. Figure 2 shows interplanetary and geomagnetic conditions during an intense space weather event of 03-04 November 2021. Figure 2 shows, from the top, (a) variations of solar wind dynamic pressure (Pdyn, red), proton density (Np, black); (b) solar wind velocity

(Vsw); (c) the y and z-components of interplanetary magnetic field (IMF), By (blue) and Bz (red); (d) the dawn-dusk component of interplanetary electric field (IEF), Ey, calculated from Ey $= (-Vx \times Bz)$; (e) the symmetric component of the ring current (Sym-H) demonstrating the evolution of magnetic storm; (f) the variation of equatorial electrojet (EEJ, blue) along with quiets days mean variation (black), EEJ calculated by subtracting the H-component from equatorial to off equatorial station (EEJ = $H_{GUA}$-$H_{KNY}$); and (g) Kp indices, which describes the global geomagnetic disturbances. The vertically shaded region indicates the main phase of the storm, in which significant changes occurred in interplanetary and geomagnetic conditions. Sudden storm commencement (SSC) occurred at 20:30 UT on November 03, and Sym-H value reached its maximum of +45 nT at 21:00 UT. In addition, the corresponding sudden increased in Pdyn, Np, and Vsw were observed with reaching from ~1 to 20 nPa, ~1 to 20 $cm^{-3}$, and ~450 to 750 $km\ s^{-1}$, respectively. At the same time, IMF Bz turned southward direction and reached up to $-15$ nT. Since the main phase of the magnetic storm had started at 21:30 UT on November 3, Sym-H reached its minimum value of ~$-117$ nT on November 4 at 12:00 UT. The recovery phase started after 12:00 UT on November 4, lasting for a few days. In the shaded region, IMF Bz shows bipolar fluctuations (from positive to negative and negative to positive) between $\sim \pm 15$ nT, and oscillation periods are between ~ 0.5 to 2 hours. Each negative (southward) and positive (northward) turning of the Bz correspond to an enhancement (duskward) and reduction (dawnward) of IEFy, respectively. During the main phase of the magnetic storm, the Kp value reached ~7.

### 3.2 GPS TEC and Ionosonde Observations

To study the TEC variations due to the present geomagnetic storm on November 4, 2021, ten GPS stations are selected over the East Asian sector between 110° -150° E longitudes, and a meridional chain of GPS receivers from high to equatorial latitudes. To compare any differences between geomagnetically quiet and disturbed days, Figures 3a-j show VTEC variations from the equator to high latitudes in the period of November 3-5, 2021. The VTEC during disturbed period is presented in solid red color lines, the average VTEC value of five international quiet days (IQDs) (IQD's are the days where the geomagnetic variations are a minimum in each month) in black solid lines, and the standard deviation of five IQDs in gray bands. During November 2021, the five IQDs are 11, 12, 13, 14, and 26. The vertically shaded areas (blue) show multiple enhancements of VTEC compared to the mean on quiet days during the main phase of the storm. It is very useful to highlight the occurrence of positive and negative ionospheric storm effects by comparing VTEC between quiet and disturbed days. Here, the disturbed VTEC clearly demonstrates three strong positive ionospheric storms with the three peaks. In the disturbed period, the VTEC takes sudden enhancements and wavelike oscillations from equatorial to high latitude regions (from -6.67-71.63$^o$ N GLat.), differentiated from the usual diurnal variation in a quiet condition. The first positive storm peak occurred at 00:30 UT (up to ~ 43.79$^o$N GLat.), the second peak at ~04:30 UT (up to ~ 62.03$^o$N GLat.), and the third peak at ~09:30 UT (up to ~ 71.63$^o$N GLat.) as indicated with blue dashed vertical lines, and other multiple peaks are also observed in between with low strengths. The multiple peaks of VTEC occur almost at the same time with different strengths from the equator to high latitudes during the entire main phase of the storm from ~21:00 UT on 03$^{rd}$ to ~12:00 UT on 04$^{th}$ November. The almost simultaneous enhancements of VTEC occurring from the low to mid latitudes are attributed to the meridional effects of the PPEF, rather than to TID or any other sources. The VTEC variations at high latitude stations at TIXI and YAKT do not synchronize with those of lower latitude stations. At high latitudes, along with the PP electric field, other magnetospheric and ionospheric disturbances (e.g., particle precipitation, auroral heating, etc.) also may play a role in modifying the high latitude ionospheric electrodynamics. In the meanwhile, the enhancements/reductions (positive/negative storm) in VTEC were also observed in the recovery phase of the magnetic storm on 04-05$^{th}$ November. The simultaneous occurrence of positive ionospheric storm at the mid-equatorial latitudes strongly implies the PP electric field-induced perturbations, while the sequential occurrence from mid-latitude first and then to low and equatorial latitudes suggests the association with DD electric field or other sources (Lima et al., 2004; Fagundes et al., 2016).

It is noticed from Figure 3 that the positive ionospheric storm peaks are not similar strengths at all latitudes. In Figure 4 the maps of (a) GPS TEC and (b) deviations of TEC (ΔTEC) are shown with universal time and geographical latitudes (-70~70$^o$N) for an East Asian Sector at ~130$^o$ E $\pm$ 20$^o$ longitudes on November 3-5, 2021. Here ΔTEC = (TEC- mean ($TEC_{IQDs}$)) is the absolute difference of TEC from the five IQDs mean during the month of November. From Figure 4a, it is clearly noticed that the Equatorial Ionization Anomaly (EIA) is significantly enhanced, and two crests of EIA extend toward the higher latitudes during the main phase on November 4. In the recovery phase, EIA crests are significantly suppressed or absent for November 5. In Figure 4, at ~ 00:30 UT on Nov. 4, significant enhancement was observed from low to high latitudes (up to ~50$^o$ N GLat). Another significant increase occurred from low to high latitudes (up to ~65° N GLat) between ~03:00 and 07:00 UT, and between ~07:00 and 12:00 UT enhancements were observed in TEC up to mid latitudes. Figure 4b displays the significant multiple enhancements in terms of ΔTEC, as indicated by p1, p2, and p3 that occurred simultaneously from the equator to high latitudes (~70° N GLat) in the northern hemisphere on November 4. The ΔTEC increase was more pronounced in the northern hemisphere than in the southern hemisphere. The simultaneous positive ionospheric storm perturbations from the equator to higher latitude regions can be related to the strong penetration of polar convective electric field. During the recovery phase on November 5, the ΔTEC shows reductions (negative ionospheric storm, indicated by n1 and n2) at low latitudes in the northern and southern hemispheres. The suppression of EIA crest or negative ionospheric storms in the northern and southern hemispheres can be associated with DD electric field disturbances.

To investigate the meridional features of the F-region over the East Asian sector a latitudinal chain of ionosondes is used. Figure 5 displays the variations of critical frequency of the F2 layer (foF2) from the equator to higher latitude stations at GUA, SA, WU, JJ, ICN, BP, and MH between 18:00 UT on November 3-23:59 UT on November 4. In Figures 5a-g, the variations of foF2 during the storm days are plotted in red lines, and the mean value and standard deviation of quiet days at respective stations are overlapped in grey lines including error bars. In Figures 5a-g, it can be clearly seen the pronounced enhancements/reductions of foF2 are observed at all stations in the main phase between ~21:00 UT on November 3 and 12:00 UT on November 4. The vertical green and blue shaded regions indicate the simultaneous enhancements of foF2 from the equator to higher latitude stations. However, in the recovery phase, foF2 shows density fluctuations with time delay from higher to lower latitudes as indicated by the blue color dashed line. The first peak in density observed at high latitude station at MH ~12:30 UT and after ~2.5 hrs reached at equatorial station at GUA ~15:00 UT. In the main phase, repeated enhancements of foF2 is typical for the events of PP electric fields, however, in the recovery phase density oscillations can be associated with DD electric field [Lima et al., 2004; Liu et al., 2014; Fagundes et al., 2016]. The signature of DD electric field can be observed in h’F. In Figures 6a-e grey lines with error bars indicate the temporal variations of mean h’F at GUA, WU, ICN, BP, and MH for quiet days. The vertically shaded region (grey) represents the main phase of the storm. During the main phase, h’Fs at all stations show normal behavior without reflecting a significant storm effect. In the meanwhile, at the equatorial station GUA height shows multiple oscillations with a large enhancement at 03:00

UT and 09:00 UT. In the recovery phase from ~12:00-21:00 UT the multiple peaks of h'F with significant changes are observed with time delay. From the figure, the ionospheric height enhancements can be seen first at the high latitude station (MH) and after ~2.5 hrs delay such enhancement can be seen over the equatorial station (GUA), as shown with blue color dashed lines. Based on the peak occurrence of h'F and foF2, the propagation speed of disturbances was calculated to give a result of time delay (~2.5 hrs) for the distance between two stations of MH and GUA (~4300 km). The phase propagation speed of disturbance is ~477 m/sec, which matches with the characteristics of TIDs [Afraimovich et al., 2002; Lima et al., 2004; Lee et al., 2004]. Generally, the horizontal wavelength of TIDs varies from 100-1000 km with the periods ranging from few minutes to hours and propagation speed ranged from 50-1000 m/sec. During the magnetic storm time, TIDs may be generated due to a large amount of energy deposition and joule heating, and they can propagate towards the low latitude from high latitude with reduced amplitudes due to the ion drag dissipation. The subsequent enhancements of ionospheric height can be associated with the strong eastward DD electric fields or TIDs as suggested by Lima et al. (2004), and Ram Singh and Sripathi. (2017, 2021).

### 3.3 Cross-correlation analysis between IEF and ionospheric parameters

The cross-correlation analysis technique can provide a measure of the similarity between different variables along with time delay. The range of cross-correlation coefficient varies from -1 to +1. The highest value of correlation between the compared parameters reflects by ±1, but moderate or poor correlation indicates by around zero. We used cross-correlation analysis technique to understand the causal relationship between solar wind parameters (e.g., IEFy) and ionospheric parameters (e.g., EEJ, H-component and VTEC). The horizontal component H of magnetic field (cf., northward in the equator) along the meridional chain of magnetometers can provide insights of the effects of the DP2 current system penetrating up to equatorial latitudes. The ΔH components are coherently fluctuating meridionally from high-mid to equatorial latitudes in good correlations with IMF Bz fluctuations so that H-components are enhanced when IMF Bz turns maximum in southward direction as shown in Figure S1 (provided as supplements).

Figure 7 shows residual variations (top panels) and cross-correlation (bottom panels) of (a) IEFy and H-components (at MGD, BMT, KAK, and GUA), (b) IEFy and EEJ, and (c) EEJ and VTEC (at BJFS, TCMC, and PIMO) during the main phase of storm from 22:00 UT on 03$^{rd}$ to 06:00 UT on 04$^{th}$ November. The residuals of all the parameters are extracted by using the 3rd order Savitzky-Golay smoothing algorithm (Savitzky and Golay, 1964).

In Figure 7a, the cross-correlation between the IEFy and H-components in MGD (black curve), BMT (green curve), and KAK (pink curve) shows good correlation with a correlation coefficient at 0.53 and a 0 time delay. In the meanwhile, the IEFy and H-component at the equatorial station (GUA) showed a maximum positive correlation coefficient of ~0.56 with a −12 min lag, which means that IEFy led the H-component 12 min before the equatorial magnetometer was triggered. In Figure 7b, IEFy and EEJ showed a maximum correlation coefficient of ~0.68 with a −12 min lag. In Figure 7c, the EEJ and VTEC at PIMO (blue curve) and TCMC (pink curve) reached positive correlations with maximum coefficients of ~0.34 and 0.63 (highest) and around zero lags, respectively; In the meanwhile, the EEJ and VTEC at BJFS (green curve) over mid latitude showed positive correlation with a maximum coefficient of ~0.40 with −7 min lag. As a result, the IEFy-H components and IEFy-EEJ gained good cross-correlations with ~0.53 and 0.68 correlation coefficients. This means that the modulations of H-components and EEJ can be associated as much as ~53% and 68% with IEFy fluctuations, respectively. The EEJ-VTEC correlation reflects that the fluctuations of VTEC at equatorial and low latitudes are moderately (~40%) affected by EEJ, while, at the mid latitude are well modulated (~68%) by EEJ.

### 3.4 Periodogram Analysis of Solar Wind/Ionospheric Parameters

To understand the causal relationship among the modulations of H-component of the magnetic field, ionospheric density (GPS-TEC and foF2) and height (h'F), and the oscillation of IEFy, we performed morlet wavelet analysis (Torrence and Compo, 1998). The fast and short fluctuating components are extracted by the Savitzk-Golay algorithm (Savitzky & Golay, 1964). Figure 8a shows the wavelet spectrum of ΔH-components at MGD (high latitude), MMB (mid latitude), KNY (low latitude) and KAK (equator). The wavelet spectrum of VTEC is shown in Figure 8b, from the top, for YAKT (high latitude), BJFS (mid latitude), TCMS (low latitude), and PIMO (equator). Figure 8c shows the wavelet spectrum of foF2 at Icheon (mid latitude), foF2 at Guam (low latitude), h'F at Guam, and IEFy. The white color dotted lines in the left panels show cones of influence; and in the right panel blue and red color lines depict the global wavelet spectrum (GWS) and 95% significant level, respectively. From the GWS, it is clear that a periodicity of ~1.05 hrs with FWHM (full width at half maximum) ~0.68-1.43 hrs is strongly dominant in H-components, VTEC, foF2 and h'F; and a dominant periodicity of ~0.9 hrs with of FWHM 0.5-1.3 hrs is obtained from IEFy. From the wavelet analysis, it is striking that the wavelet analysis finds a common and dominant periodic oscillation of ~1 hr period in the IEFy and ionospheric parameters. This analysis suggests that the perturbations of ionospheric density and magnetic field are the result of being modulated by quasi-periodically oscillating penetrating electric field or reorientation of the IMF Bz.

## 4. Discussion:

It is well known that the orientations of IMF Bz most strongly control the energy transfer into the magnetosphere-ionosphere system. During the southward turning of IMF Bz, enhanced magnetospheric convection electric field penetrates into the equatorial and low latitude ionospheres via the high-latitude DP2 current system (Nishida, 1968; Araki et al., 1985; Kikuchi et al., 1996; Huang 2019a, 2020), and significantly changes the electrodynamics and compositions in the lower latitude ionospheric regions (Reddy et al., 1990; Kelley et al., 2004, Lima et all., 2004; Lin et al., 2005; Balan et al., 2010; Ram Singh et al., 2015; Fagundes et al., 2016).

### 4.1 Ionospheric density modulation by PPEF and TID

Fagundes et al., (2016) have reported that the positive ionospheric peaks occurred simultaneously at mid and low latitude regions over the Brazilian sector on 17 March 2015. They suggested that the simultaneous enhancements of electron density peaks or wavelike oscillations in electron density are strongly associated with PPEFs, but not by the traveling ionospheric disturbances (TIDs) or other sources. Our observations (Figures 3-5) show simultaneous modulations in the electron density (TEC/foF2) during the main phase of the storm on November 04. The repeated enhancements at all stations over the East Asian sector are believed to be due to the PPEFs. The plausible scenario for this interpretation goes as following: the electric field penetrates meridionally at all latitudes and uplifts the ionospheric F region to higher altitudes, where the recombination rates are much lower, resulting in enhancements of electron density.

Lima et al. (2004) distinguished the role of electric field from TIDs on the positive ionospheric storms along the meridional direction. They suggested that, in the case of TIDs, the perturbations are first observed at mid latitudes or beyond the EIA crest and then at low latitudes and finally at the equatorial region. However, as for the PP electric field, the positive ionospheric storm perturbations must simultaneously occur at all latitudes, since the PP electric field is on the global scale.

During the recovery phase of the magnetic storm, on 04-05th November, enhancements and reductions in foF2 are due to DD electric fields or TIDs (Figure 5). The first peak in ionospheric density observed at high latitude station and after ~2.5 hours occurred at the equator with propagation speed ~477 km/sec, as pointed out with blue color dashed line (in Figure 5). Since we see some correlation between one station and others with a time delay, we believe that they could be due to the TIDs or DDEFs. On 5 November, suppression of EIA crest or negative ionospheric storm at low latitudes may be linked to the DDEF (Figure 4).

### 4.2 h’F modulation by PPEF and TIDs (or DDEF)

Ram Singh and Sripathi (2017) showed the simultaneous reductions/enhancements in h’F over the Indian region using a chain of ionosondes. They suggested that the ionospheric F region disturbances during the main phase of the storm are produced by the PPEF. It has been suggested that the super fountain effect during the geomagnetic storm is closely linked with PPEF and it leads to a stronger EIA (Lu et al., 2012; Abdu et al., 2007; Mannucci et al., 2005, Ram Singh et al., 2017). Our observations clearly show that EIA over the East Asian sector is significantly affected by the PPEF, and extending the enhanced electron density to higher latitudes. Meanwhile, several authors have also suggested that the storm time enhancement and suppression in the foF2 at midlatitudes are due to the change of thermospheric compositions (Prolss, 1977; Rishbeth, 1975), and wavelike disturbances in foF2 associated with high velocity TIDs or with substorm activity (Turunen and Mukunda Rao., 1980; Lima et al., 2004).

Sastri et al. (2000) presented the sharp reductions/enhancements of F layer height (h’F) at the same time at several stations over the Indian region, and suggested that reductions/enactments of F layer height are associated with the westward/eastward penetration electric fields. During the recovery phase of the magnetic storm, Figure 6 shows TID signature so that the first peaks of the h’F first observed at the high latitude stations and after ~2.5 hours reached at the equator, as pointed out with blue color dashed lines. Since we see a systematic enhancement along the h’F stations with a time delay (slope = 477 m/s), we believe that they could be associated with TIDs.

### 4.3 Evidence of oscillations of PPEF and DP2 current system

It is well established that the PPEF is linked to the region 1 (R1) and region 2 (R2) field-aligned currents and their horizontal closure currents, and they play an important role in generating the global scale ionospheric currents. When the FACs are in their dynamical activities, they can generate significant fluctuations in DP2 current systems that can easily penetrate to the equatorial region and modulate the electrodynamics of the ionosphere. Several studies have focused on the formations of quasi-periodic ionospheric current systems (Nishida 1968a, 1968b; Huang, 2019a, 2020), and solar wind magnetosphere-ionosphere coupling processes (Kikuchi et al., 1996; Kamide et al., 1997, 1998) and their impacts on the equatorial density distribution (Yizengaw et al., 2016; Rodriguez et al., 2016). The quasi-periodic disturbances in ionospheric current systems are associated with various solar wind and magnetospheric processes (Nishida 1968a, 1968b; Kikuchi et al., 2000; Motoba et al., 2003; Huang, 2019a). Nishida (1968a, 1968b) reported the quasi-periodic oscillations in geomagnetic field measured by the ground-based magnetometers near the magnetic equator, caused by the penetration of electric fields associated with turning of IMF Bz with periods ~30-60 min. They suggested that during the turning of IMF Bz (north-south), the convection electric field and DP2 currents enhances and causes the magnetic fluctuations at the equator through the penetration electric field. Gonzales et al., (1979) and Earle and Kelley (1987) reported the significant dominance of 1-hour periodicity in the IMF Bz as well in the electric fields at the auroral and equatorial latitudes. In our observations, magnetic field perturbations at high mid and low latitudes are well correlated with reorientations of IMF Bz (Figure S1) and show common and dominant periods ~30 to 90 min (Figure 8).

In a recent study, Huang (2019a) analyzed the observations of equatorial ionospheric plasma drift measured by the Jicamarca incoherent scatter radar and global ground magnetic field perturbations during IMF Bz fluctuations. Huang (2019a) also reported that the vertical plasma drifts/zonal electric fields in the dayside equatorial ionosphere are well correlated with reorientations of IMF Bz. Using the combination of ground-based magnetometers and EISCAT radar data, Kikuchi et al., (2000) showed a significant increase/decrease of the DP2 current system at high latitude and EEJ at the equator, according to sudden polarity changes of IMF Bz from north-south/south-north. They suggested that when IMF Bz turns north-south/south-north both the DP2 current system and EEJ get enhanced/decayed, and eastward/westward electric field enhanced/reduced at the equator. The correlations coefficient of IEFy with EEJ and H-components is 0.68 and 0.53, respectively, suggesting that the IEFy is playing an important role in electric field penetration down to the equatorial region. Our observations show excellent time coincidence between the IMF Bz minimum and H-components peaks

(Figure S1), the H-components enhanced when IMF Bz turns maximum in southward direction which are consistent results as presented in the previous studies (Kikuchi et al., 2000; Yizengaw et al., 2016; Huang, 2019a, 2020).

In general, the vertical motion of the ionosphere is driven by the eastward/westward electric field at the equator, which generates due to the turning of IMF Bz. As shown in Figure 7, the correlation of a latitudinal array of H-components with IMF Bz can be an evidence of the modulated DP2 currents to be effective on all the latitudes in the longitudinal sector. Given this correlation, the coherent fluctuations of the VTEC/foF2 (in Figures 3 and 5) can be the signatures in the lower latitude ionosphere affected by the modulated DP2 current system. Figure 6 shows that the virtual height of the ionosphere is not showing pronounced effect of storm at all latitudes, but oscillating up and down compared to mean variation at equatorial and low latitudes, implying that the DP2 current fluctuations control the ionospheric F-layer height. This can be demonstrate that the magnetospheric origin quasi-periodic electric field can penetrate to the ionosphere and drive DP2 current fluctuations that extend to the lower latitude ionosphere and create significant effects on the ionospheric density distribution by making the F layer move up and down. The correlation between the magnetospheric origin electric fields measured by the ground-based magnetometers and those by radars during magnetic storm periods have been performed (Kelley et al., 2007; Wei et al., 2008; Yizengaw et al., 2016). In addition, several researchers have reported a wide range of periodicities of ~0.5 to 2 hours associated with the DP2 current system (Nishida 1968a, 1968b; Gonzales et al., 1979; Earle and Kelley, 1987; Sastri et al., 2002; Motoba et al., 2003; Chakrabarty et al. 2008; Huang, 2019a, Ram Singh and Sripathi., 2021). Nonetheless, we report that the solar wind-magnetosphere-ionosphere interactions-driven DP 2 current systems can modulate ionospheric density not only at the equatorial latitude, as did by Yizengaw et al. (2016), but also, for the first time, at high-mid and low latitudes. Based on the wavelet analysis we also report a dominant periodicity of ~1 hr VTEC, foF2 and H-component, which are driven by the PP electric field associated with the DP2 current system due to IMF Bz. This suggests a causal relationship exists among IEF, DP2 current system, and ionospheric density oscillations at all latitudes.

## 5. Conclusions

This study observed the meridional ionospheric density responses to prompt penetration electric field (PPEF) over the East Asian sector, during an intense geomagnetic storm that occurred on November 3-5, 2021 in the current solar cycle 25. The important findings of the investigation can be summarized as follows:

(1) The VTEC and foF2 observations demonstrated that repeated positive ionospheric storms can be associated with reorientations of IMF Bz or DP2 current systems.

(2) From the time-latitude map of TEC observation, the equatorial ionization anomaly (EIA) is significantly disturbed during the main phase, and the signature of repeated positive ionospheric storms are observed. It is remarkable that three peaks of VTEC/foF2 with large amplitudes are extended from the equator to high latitudes simultaneously without wave propagation signatures. The first peak occurred at $6.67^{o}$ S-$43.79^{o}$ N, the second peak with a large amplitude in the extended latitude range of $6.67^{o}$ S-$62.03^{o}$ N, and the third peak in $14.67^{o}$ S-$71.63.79^{o}$ N.

(3) In the recovery phase, enhancements/reductions in foF2 and h'F are associated with the disturbance dynamo (DD) electric field or traveling ionospheric disturbances (TIDs).

(4) The periodogram analysis and wavelet spectra show dominant and common periods of ~1 hour among VTEC, H-component, foF2, h'F, and IEFy.

We conclude that the modulations of VTEC, foF2 and H-component during the main phase of geomagnetic storm can be driven by the PP electric field associated with DP2 current system and IMF Bz, and in the recovery phase, the response of VTEC from equatorial to mid latitudes can be driven by DD electric field or TIDs. The common and dominant periodicity of 1hr in all the ionospheric parameters and IEF suggests that a causal relationship exists among IEF, DP2 current system, and ionospheric density modulations at all latitudes.

**Acknowledgments**

This work was supported by the National Research Foundation of Korea (NRF) grant funded by the Korea government (MSIP) (No. 2021R1A2C1005306). We acknowledge use of NASA/GSFC's Space Physics Data Facility's OMNIWeb (or CDAWeb or ftp) service, and OMNI data used in this study. The VTEC-GPS data were obtained through the online archives of the Crustal Dynamics Data Information System (CDDIS), NASA Goddard Space Flight Center, Greenbelt, MD, USA, and from MIT Haystack Observatory Madrigal database.

## References


Abdu, M. A. (1997). Major phenomena of the equatorial ionosphere-thermosphere system under disturbed conditions. *J. Atmos. Sol. Terr. Phys.*, 59, 1505–1519.

Abdu, M. A., Maruyama, T., Batista, I. S., Saito, S., & Nakamura, M. (2007). Ionospheric responses to the October 2003 superstorm: Longitude/local time effects over equatorial low and middle latitudes. *J. Geophys. Res.*, 112, A10306. https://doi.org/10.1029/2006JA012228.

Abdu, M. A., Sastri, J. H. et al. (1998). DP 2 electric field fluctuations in the dusk-time dip equatorial ionosphere. *Geophys. Res. Lett.*, 25(9), 1511–1514.

Afraimovich, E. L., et al. (2002). Simultaneous radio and optical observations of the mid-latitude atmospheric response to a major geomagnetic storm of 6-8 April 2000. *J. Atmos. Sol. Terr. Phys.*, 64, 1943–1955.

Araki, T., J. H. Allen, & Y. Araki (1985). Extension of a polar ionospheric current to the night side equator. *Planet. Space Sci.*, 33(1), 11–16.

Balan, N., K. Shiokawa, Y. Otsuka, et al. (2010). A Physical mechanism of positive ionospheric storms at low and mid latitudes through observations and modelling. *J. Geophys. Res.*, 115, A02304, doi:10.1029/ 2009JA014515.

Blanc & Richmond (1980). the ionospheric disturbances dynamo. *J. Geophys. Res.*, 85, 1669.

Chakrabarty, D., R. Sekar, J. H. Sastri, & S. Ravindran (2008). Distinctive effects of interplanetary electric field and substorm on nighttime equatorial F layer: A case study. *Geophys. Res. Lett.*, 35 (19), 307 doi:10.1029/2008GL035415, l19108.

Clauer, C. R., & Y. Kamide (1985). DPl and DP2 current systems for the March 22, 1979 substorms. *J. Geophys. Res.*, 90, 1343–1354.

Earle & Kelley (1987). Electric Field Strength, Fourier Analysis, Incoherent Scatter Radar, Ionospheric Currents, Spectrum Analysis, Gravity Waves, Periodic Variations, Plasma Drift. *J. Geophys. Res.*, 10.1029/JA092iA01p00213.

Fagundes, P. R., F. A. Cardoso, B. G. Fejer, et al. (2016). Positive and negative GPS-TEC ionospheric storm effects during the extreme space weather event of March 2015 over the Brazilian sector. *J. Geophys. Res.*, 121, 5613–5625, doi:10.1002/2015JA022214.

Fujiwara, H., Maeda, S., Fukunishi, H., Fuller-Rowell, T.J., & Evans, D.S. (1996). Global variations of thermospheric winds and temperatures caused by substorm energy injection. *J. Geophys. Res.*, 101, 225–239.

Fuller-Rowell, T. J., Codrescu, M. V., Rishbeth et al. (1996). On the seasonal response of the thermosphere and ionosphere to geomagnetic storms. *J. Geophys. Res.*, 101(A2):2343-2353.

Gaunt, C. T. & Coetzee, G. (2007). Transformer failures in regions incorrectly considered to have low GIC-risk. *IEEE Lausanne Power Tech*, pp. 807-812, doi: 10.1109/PCT.2007.4538419.

Goncharenko, L. P., J. C. Foster, A. J. Coster, C. Huang, N. Aponte, & L. J. Paxton (2007). Observations of a positive storm phase on 10 September 2005. *J. Atmos. Sol. Terr. Phys.*, 69 (10–11), 1253–1272, doi: 10.1016/j.jastp.2006.09.011.

Gonzales, C. A., Kelley, M. C., & Woodman, R. F. (1979). Equatorial electric fields during magnetically disturbed conditions: Implications of simultaneous auroral and equatorial measurements. *J. Geophys. Res.*, 84, 5803–5812.

Huang, C.-S. (2019a). Global ionospheric current system associated with penetration electric field and new mechanism for the generation of dayside westward electric field at low latitudes during northward IMF. *J. Geophys. Res.*, 124, 3827–3842. https://doi.org/10.1029/2018JA026345.

Huang, C.-S. (2020). Systematical analyses of global ionospheric disturbance current systems caused by multiple processes: Penetration electric fields, solar wind pressure impulses, magnetospheric substorms, and ULF waves. *J. Geophys. Res.*, 125, e2020JA027942. https://doi.org/10.1029/2020JA027942.

Joshi, L. M., S. Sripathi, & R. Singh (2016). Simulation of low-latitude ionospheric response to 2015 St. Patrick's Day super geomagnetic storm using ionosonde-derived PRE vertical drifts over Indian region. *J. Geophys. Res.*, 121, 2489–2502, doi:10.1002/2015JA021512.

Kamide, Y., Baumjohann, W., Daglis, I. A. et al. (1998). Current understanding of magnetic storms: Storm-substorm relationships. *J. Geophys. Res.*, 103, 17,705–17,728. https://doi.org/10.1029/98JA01426.

Kamide, Y., McPherron, R. L., Gonzalez, W. D. et al. (1997). Magnetic storms: Current understanding and outstanding questions. In B. T. Tsurutani, et al. (Eds.), Magnetic Storms (pp. 1–19). *Washington, DC: American Geophysical Union*. https://doi.org/10.1029/GM098p0001.

Kelley, M. C., Fejer, B. G., & Gonzalez, C. A. (1979). An explanation for anomalous equatorial ionospheric electric fields associated with the northward turning of the interplanetary magnetic field. *Geophys. Res. Lett.*, 6(4), 301–304.

Kelley, M. C., M. J. Nicolls, et al. (2007). Multi-longitude case studies comparing the interplanetary and equatorial ionospheric electric fields using an empirical model. *J. Atmos.*

*Terr. Phys.*, 69(10–11), 1174–1181, doi: 10.1016/j.jastp.2006.08.014.

Kelley, M. C., M. N. Vlasov, J. C. Foster, & A. J. Coster (2004). A quantitative explanation for the phenomenon known as storm-enhanced density. *Geophys. Res. Lett.*, 31, L19809, doi:10.1029/2004GL020875.

Kikuchi, T. (1986). Evidence of transmission of polar electric fields to the low latitude at times of geomagnetic sudden commencements. *J. Geophys. Res.*, 91(A3), 3101–3105.

Kikuchi, T., K. K. Hashimoto, & K. Nozaki (2008). Penetration of magnetospheric electric fields to the equator during a geomagnetic storm. *J. Geophys. Res.*, 113, A06214, doi:10.1029/2007JA012628.

Kikuchi, T., Luhr, H. et al. (2000). Penetration of auroral electric fields to the equator during a substorm. *J. Geophys. Res.*, 105(A10), 23,251–23, 261.

Kikuchi, T., Lühr, H., Kitamura, T. et al. (1996). Direct penetration of the polar electric field to the equator during a DP 2 event as detected by the auroral and equatorial magnetometer chains and the EISCAT radar. *J. Geophys. Res.*, 101(A8), 17,161–17,173.

Lee, C. C., J. Y. Liu, M. Q. Chen, S. Y. Su, H. C. Yeh, & K. Nozaki (2004). Observation and model comparisons of the traveling atmospheric disturbances over the Western Pacific region during the 6–7 April 2000 magnetic storm. *J. Geophys. Res.*, 109, A09309, doi:10.1029/2003JA010267.

Lima, W. L. C., F. Becker-Guedes, et al. (2004). Response of the equatorial and low-latitude ionosphere during the space weather events of April 2002. *Ann. Geophys.*, 22(9), 3211–3219, doi:10.5194/angeo-22-3211-2004.

Lin, C. H., A. D. Richmond, R. A. Heelis, G. J. Bailey, G. Lu, J. Y. Liu, H. C. Yeh, & S. Y. Su (2005). Theoretical study of the low-and midlatitude ionospheric electron density enhancement during the October 2003 storm: Relative importance of the neutral wind and the electric field. *J. Geophys. Res.*, 110, A12312, doi:10.1029/2005JA011304.

Liu, C. M., L. G. Liu, R. Pirjola, & Z. Z. Wang (2009). Calculation of geomagnetically induced currents in mid- to low-latitude power grids based on the plane wave method: A preliminary case study. *Space Weather*, 7, S04005, doi:10.1029/2008SW000439.

Liu, J., L. Liu, T. Nakamura, B. Zhao, B. Ning, & A. Yoshikawa (2014). A case study of ionospheric storm effects during long-lasting southward IMF Bz-driven geomagnetic storm. *J. Geophys. Res.* 119, 7716–7731, doi:10.1002/2014JA020273.

Lu, G., L. Goncharenko, M. J. Nicolls, A. Maute, A. Coster, & L. J. Paxton (2012). Ionospheric and thermospheric variations associated with prompt penetration electric fields. *J. Geophys.*

*Res.*, 117, A08312, doi:10.1029/2012JA017769.

Mannucci, A. J., Tsurutani, B. T., Iijima, et al. (2005). Dayside global ionospheric response to the major interplanetary events of October 29–30, 2003 “Halloween storms”. *Geophys. Res. Lett.*, 32, L12S02. https://doi.org/10.1029/2004GL021467.

Motoba, T., Kikuchi, T., Okuzawa, T., & Yumoto, K. (2003). Dynamical response of the magnetosphere-ionosphere system to a solar wind dynamic pressure oscillation. *J. Geophys. Res.*, 108(A5), 1206.

Nishida, A. (1968a). Geomagnetic DP 2 fluctuations and associated magnetospheric phenomena. *J. Geophys. Res.*, 73(5), 1795–1803, doi: 10.1029/JA073i005p01795.

Nishida, A. (1968b). Coherence of geomagnetic DP 2 fluctuations with interplanetary magnetic variations. *J. Geophys. Res.*, 73(17), 5549–5559, doi: 10.1029/JA073i017p05549.

Noll, C.E. (2010). The Crustal Dynamics Data Information System: A resource to support scientific analysis using space geodesy. *Adv. Space Res.* 2010, 45, 1421–1440.

Prolss, G. W. (1977). Seasonal variations of atmospheric-ionospheric disturbances. *J. Geophys. Res.*, 82, 1635–1640.

Prolss, G. W. (1993). Common origin of positive ionospheric storms at middle latitudes and the geomagnetic activity effect at low latitudes. *J. Geophys. Res.*, 98(A4):5981–5991.

Prolss, G. W., Brace, L. H. and. Mayr, H. G. et al. (1991). Ionospheric storm effects at subauroral latitudes: A case study. *J. Geophys. Res.*, 96(A2):1275–1288.

Prolss, G., Roemer, M., & Slowey, J. (1988). Dissipation of solar wind energy in the earth’s upper atmosphere: The geomagnetic activity effect. *Adv. Space Res.*, (5-6):215-261.

Ram Singh & Sripathi, S. (2021). The role of storm-time electrodynamics in the dawn and dusk sectors across equatorial and low-latitude ionosphere during December 19–21, 2015. *J. Geophys. Res.*, 126, e2020JA029072.

Ram Singh, S. Sripathi, et al., (2015). Low-latitude ionosphere response to super geomagnetic storm of 17/18 March 2015: Results from a chain of ground based observations over Indian sector. *J. Geophys. Res.*, 120, 10,864–10,882.

Ram Singh., & Sripathi, S. (2017). Ionospheric response to 22–23 June 2015 storm as investigated using ground-based ionosondes and GPS receivers over India. *J. Geophys. Res.*, 122, 11,645–11,664. 2017JA024460.

Reddy, C. A., Nishida, A., Fukao, S., & Somayajulu, V. V. (1990). Magnetospheric substorm related electric fields in the ionosphere: Discrepancy of an observation with model predictions. *Geophys. Res. Lett.*, 17(13):2333–2336.

Rishbeth, H. (1975). F-region storms and thermospheric circulation. *J. Atmos. Sol. Terr. Phys.,* 37, 1055–1064. https://doi. org/10.1016/0021-9169(75)90013-6.

Rishbeth, H. (1991). F-region storms and thermospheric dynamics. *Journal of geomagnetism and geoelectricity*, 43(Supplement1):513–524.

Rishbeth, H. (1998). How the thermospheric circulation affects the ionospheric F2-layer. *J. Atmos. Sol. Terr. Phys.*, 60(14):1385–1402.

Rodriguez-Zuluaga, J., S. M. Radicella, et al. (2016). Distinct responses of the low-latitude ionosphere to CME and HSSWS: The role of the IMF Bz oscillation frequency. *J. Geophys. Res.,* 121, 11,528–11,548, doi:10.1002/2016JA022539.

Sastri, J. H., Abdu, M. A., Batista, I. S., & Sobral, J. H. A. (1997). Onset conditions of equatorial (range) spread F at Fortaleza, Brazil, during the June solstice. *J. Geophys. Res.,* 102, 24,013–24,021.

Sastri, J. H., Jyoti, N., Somayajulu, V. V., Chandra, H., & Devasia, C. V. (2000). Ionospheric storm of early November 1993 in the Indian equatorial region. *J. Geophys. Res.*, 105, 18,443–18,455. https://doi.org/10.1029/1999JA000372.

Sastri, J. H., Niranjan, K., & Subbarao, K. S. V. (2002). Response of the equatorial ionosphere in the Indian (midnight) sector to the severe magnetic storm of July 15, 2000. *Geophys. Res. Lett.,* 29(13), 1651.10.10292002/2002GL015133.

Savitzky, A., & Golay, M. J. E. (1964). Smoothing and differentiation of data by simplified least squares procedures. *Analytical Chemistry*, 36, 1627– 1639. doi.org/10.1021/ac60214a047.

Spiro, R. W., Wolf, R. A., & Fejer, B. G. (1988). Penetration of high-latitude-electric-field effects to low latitudes during SUNDIAL 1984. *Annales de Geophysique,* 6, 39–50.

Torrence, C., and G. P. Compo (1998). a practical guide to wavelet analysis, Bull. *Am. Meteorol. Soc*.79, 61-78.

Turunen, T., & Mukunda Rao, M. (1980). Examples of the influence of strong magnetic storms on the equatorial F-layer. *J. Atmos. Sol. Terr. Phys.,* 42, 323–330.

Wei, Y., M. Hong, W. Wan, A. Du, J. Lei, et al. (2008). Unusually long-lasting multiple penetration of interplanetary electric field to equatorial ionosphere under oscillating IMF Bz. *Geophys. Res. Lett.,* 35, L02102, doi:10.1029/2007GL032305.

Yizengaw, E., Moldwin, M. B., Zesta, E., Magoun, M., Pradipta, R., Biouele, C. M., Rabiu, A. B., Obrou, O. K., Bamba, Z., & de Paula, E. R. (2016). Response of the equatorial ionosphere to the geomagnetic DP 2 current system. *Geophys. Res. Lett.,* 43, 7364– 7372, doi:10.1002/2016GL070090.

Zhao, B., Wan, W., Lei, J., Wei, Y., Sahai, Y., & Reinisch, B. (2012). Positive ionospheric storm effects at Latin America longitude during the superstorm of 20–22 November 2003: Revisit. *Annales de Geophysique*, 30, 831–840.

**Figures:**

**Figure 1.** The location of various stations and instruments used in present study, (a) locations of GPS receivers, and Ionosondes, and (b) magnetometers.

**Figure 2.** Variation of interplanetary and geomagnetic conditions during the 03-05 November 2021. (a) Particle density (Np ($cm^{-3}$)), black) and solar wind pressure (Pdyn (nPa)), red), (b) solar wind velocity (m/sec), (c) IMF By (blue) and Bz (red) in nT, (d) IEFy (mV/m), (e) Dst (nT), (f) EEJ (nT), and (g) Kp index. The black color shaded region indicates the main phase of the storm.

**Figure 3.** The VTEC diurnal variations (red solid lines) over the East Asian sector during the 03-05 November. The grey shaded region and solid black lines show IQDs mean and the averaged standard deviation. The vertical dotted blue color lines indicate the VTEC enhancements. The p1, p2 and p3 represent positive ionospheric storms. The n1 and n2 indicate negative ionospheric storms.

**Figure 4.** Shows (a) latitudinal and temporal variations of TEC (contour map); (b) ΔTEC = ($TEC-TEC_{IQDs}$ Mean); $TEC_{IQDs}$ Mean is five IQDs variations during the November month, over the Asian sector between 110-150$^o$ E longitude.

**Figures 5.** Temporal variation of foF2 at (a) MH, (b) BP, (c) ICN, (d) JJ, (e) WU, (f) SA, and (g) GUA. The grey color lines with error bars indicate the quiet days mean and standard deviation. The vertical shaded green and blue color indicate the simultaneous enhancements in foF2.

**Figures 6.** Variations of h'F at (a) MH, (b) BP, (c) ICN, (d) WU, and (e) GUA. The grey color lines with error bars indicate the quiet days mean and standard deviation. The dashed blue color lines indicate the enhancements in h'F.

**Figure 7**. Infiltration of PPEF effects examined with cross-correlation analysis: Residual variations (top panels) and cross-correlation (bottom panels) of (a) IEFy and H-components (at MGD, BMT, KAK, and GUA), (b) IEFy and EEJ, and (c) EEJ and VTEC (at BJFS, TCMC, and PIMO) during 03-04 November 2021.

**Figure 8.** Wavelet spectrum analysis of (a) H-components of magnetic field at MGD, MMB KNY and KAK stations (top to bottom); (b) VTEC at YAKT, BJFS, TCMS and PIMO (top to bottom); and (c) foF2 ate Icheon (mid latitude) and Guam (low latitude), h'F at Guam, and IEFy (bottom panel). The dotted white color lines in each plot indicate cone of influence (COI). The rightside panels of each plot show global wavelet spectrum (GWS) with 95% confidence level (in red color).

**Table 1.** Details of the GPS TEC stations, Ionosondes, SuperDARN and Magnetometers with name, station code, latitudes and longitudes

| Location | Station CODE | Geographic (Latitude) | Geographic (Longitude) | Geomagnetic (Latitude) | Geomagnetic (Longitude) |
|---|---|---|---|---|---|
| | | | **GPS Receivers** | | |
| Tixi | TIXI | 71.63$^{o}$ N | 128.86$^{o}$ E | 61.94$^{o}$ N | 165.77$^{o}$ W |
| Yakutsk | YAKT | 62.03$^{o}$ N | 129.68$^{o}$ E | 53.06$^{o}$ N | 162.64$^{o}$ W |
| Changchun | CHAN | 43.79$^{o}$ N | 125.44$^{o}$ E | 34.64$^{o}$ N | 164.12$^{o}$ W |
| Fangshan | BJFS | 39.60$^{o}$ N | 115.89$^{o}$ E | 30.14$^{o}$ N | 172.39$^{o}$ W |
| Suwon-shi | SUWN | 37.27$^{o}$ N | 127.05$^{o}$ E | 28.23$^{o}$ N | 162.15$^{o}$ W |
| Daejeon | DAEJ | 36.39$^{o}$ N | 127.37$^{o}$ E | 27.36$^{o}$ N | 161.86$^{o}$ W |
| Hsinchu | TCMC | 24.79$^{o}$ N | 120.98$^{o}$ E | 15.53$^{o}$ N | 167.13$^{o}$ W |
| Hong kong | HKWS | 22.43$^{o}$ N | 114.33$^{o}$ E | 13.00$^{o}$ N | 173.35$^{o}$ W |
| Quezon City | PIMO | 14.63$^{o}$ N | 121.07$^{o}$ E | 05.43$^{o}$ N | 166.64$^{o}$ W |
| Lae | LAE | -06.67$^{o}$ N | 146.99$^{o}$ E | 13.78$^{o}$ S | 139.25$^{o}$ W |
| | | | **Ionosondes** | | |
| Mohe | MH | 52.00$^{o}$ N | 122.52$^{o}$E | 42.73$^{o}$N | 167.26$^{o}$W |
| Beijing | BP | 40.30$^{o}$N | 116.20$^{o}$E | 30.85$^{o}$N | 172.10$^{o}$W |
| I-cheon | IC | 37.14$^{o}$ N | 127.54$^{o}$ E | 28.11$^{o}$ N | 161.76$^{o}$ W |
| Jeju | JJ | 33.43$^{o}$ N | 126.30$^{o}$ E | 24.36$^{o}$ N | 162.64$^{o}$ W |
| Wuhan | WU | 30.50$^{o}$N | 114.40$^{o}$E | 21.04$^{o}$N | 173.46$^{o}$W |
| Sanya | SA | 18.53$^{o}$N | 109.61$^{o}$E | 08.87$^{o}$N | 177.99$^{o}$W |
| Guam | GUA | 13.69$^{o}$ N | 144.87$^{o}$ E | 06.12$^{o}$ N | 143.44$^{o}$ W |
| | | | **Magnetometers** | | |
| Magadan | MGD | 60.05$^{o}$ N | 150.72$^{o}$ E | 53.32$^{o}$ N | 139.34$^{o}$ W |
| Paratunka | PET | 52.97$^{o}$ N | 158.20$^{o}$ E | 46.36$^{o}$ N | 137.17$^{o}$ W |
| Memambetsu | MMB | 43.91$^{o}$ N | 144.19$^{o}$ E | 36.01$^{o}$ N | 147.59$^{o}$ W |
| Beijing MingTombs | BMT | 40.30$^{o}$ N | 116.20$^{o}$ E | 30.85$^{o}$ N | 172.10$^{o}$ W |
| Gangneung | GANG | 37.75$^{o}$ N | 128.87$^{o}$ E | 28.39$^{o}$ N | 161.01$^{o}$ W |
| Ichoen | ICN | 37.14$^{o}$ N | 127.54$^{o}$ E | 27.74$^{o}$ N | 161.78$^{o}$ W |
| Kakioka | KAK | 36.23$^{o}$ N | 140.18$^{o}$ E | 28.04$^{o}$ N | 150.20$^{o}$ W |
| Jeju | JEJU | 33.43$^{o}$ N | 126.30$^{o}$ E | 24.15$^{o}$ N | 162.81$^{o}$ W |
| Kanoya | KNY | 21.42$^{o}$ N | 130.80$^{o}$ E | 12.66$^{o}$ N | 157.64$^{o}$ W |
| Guam | GUA | 13.69$^{o}$ N | 144.87$^{o}$ E | 06.12$^{o}$ N | 143.44$^{o}$ W |

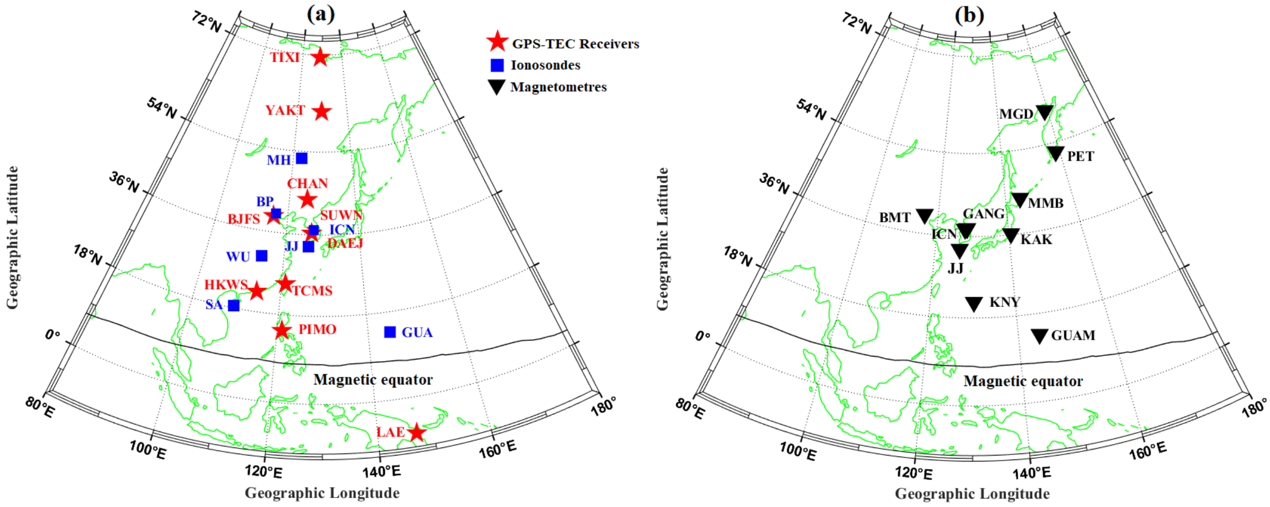
(a)
GPS-TEC Receivers
Ionosondes
Magnetometres
TIXI
YAKT
MH
CHAN
BP
BJFS
SUWN
ICN
JJ
DAEJ
WU
HKWS
TCMS
SA
PIMO
GUA
Magnetic equator
LAE
72°N
54°N
36°N
18°N
0°
80°E
100°E
120°E
140°E
160°E
180°
Geographic Latitude
Geographic Longitude
(b)
MGD
PET
MMB
BMT
GANG
ICN
KAK
JJ
KNY
GUAM
Magnetic equator
72°N
54°N
36°N
18°N
0°
80°E
100°E
120°E
140°E
160°E
180°
Geographic Latitude
Geographic Longitude

**Figures 1 (a-b)**

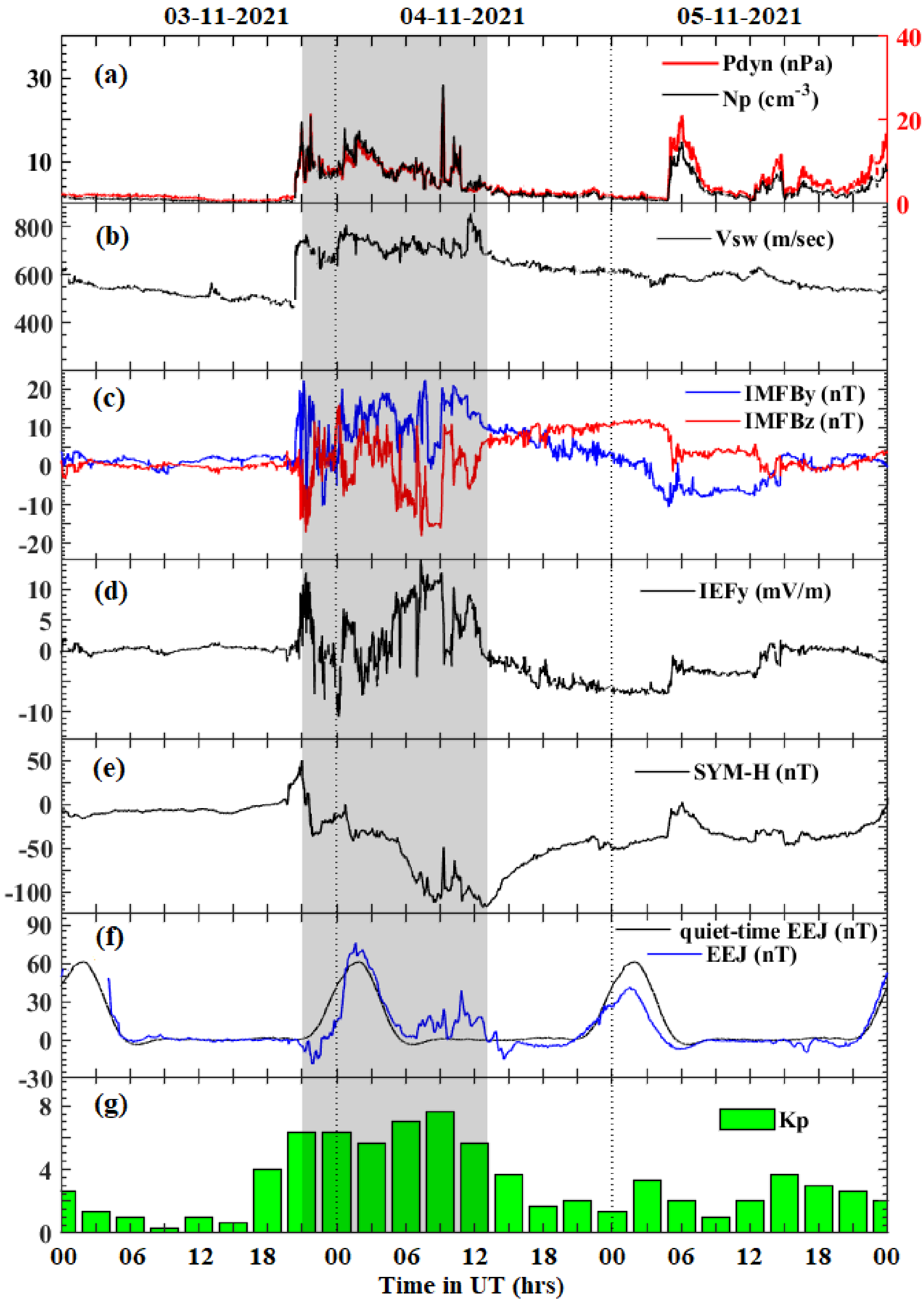
03-11-2021
04-11-2021
05-11-2021
(a)
Pdyn (nPa)
Np (cm-3)
(b)
Vsw (m/sec)
(c)
IMFBy (nT)
IMFBz (nT)
(d)
IEFy (mV/m)
(e)
SYM-H (nT)
(f)
quiet-time EEJ (nT)
EEJ (nT)
(g)
Kp
00 06 12 18 00 06 12 18 00 06 12 18 00
Time in UT (hrs)

**Figures 2 (a-g)**

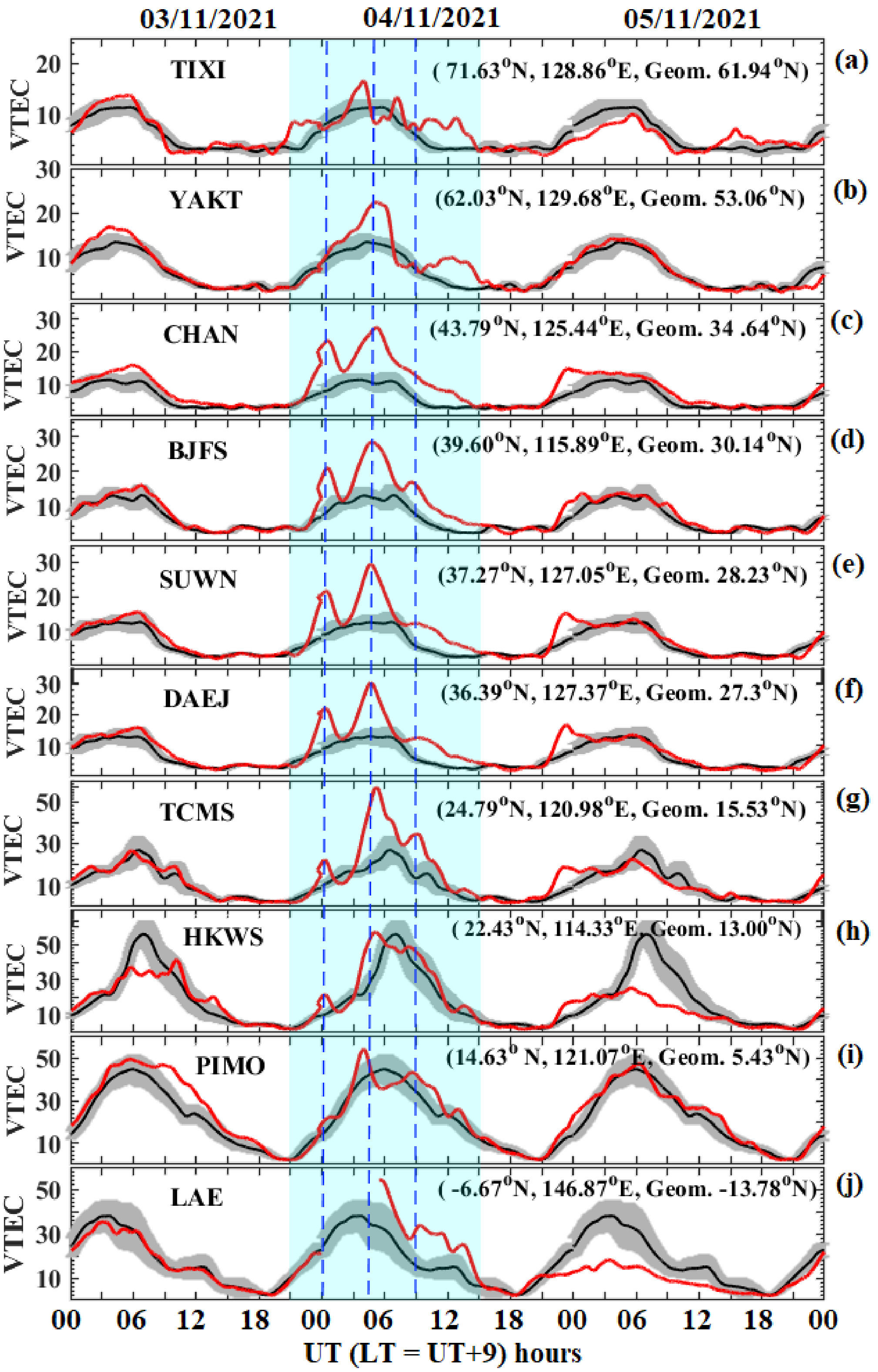
03/11/2021
04/11/2021
05/11/2021
TIXI
( 71.63°N, 128.86°E, Geom. 61.94°N)
(a)
YAKT
(62.03°N, 129.68°E, Geom. 53.06°N)
(b)
CHAN
(43.79°N, 125.44°E, Geom. 34 .64°N)
(c)
BJFS
(39.60°N, 115.89°E, Geom. 30.14°N)
(d)
SUWN
(37.27°N, 127.05°E, Geom. 28.23°N)
(e)
DAEJ
(36.39°N, 127.37°E, Geom. 27.3°N)
(f)
TCMS
(24.79°N, 120.98°E, Geom. 15.53°N)
(g)
HKWS
( 22.43°N, 114.33°E, Geom. 13.00°N)
(h)
PIMO
(14.63° N, 121.07°E, Geom. 5.43°N)
(i)
LAE
( -6.67°N, 146.87°E, Geom. -13.78°N)
(j)
VTEC
00 06 12 18 00 06 12 18 00 06 12 18 00
UT (LT = UT+9) hours

**Figure 3 (a-j)**

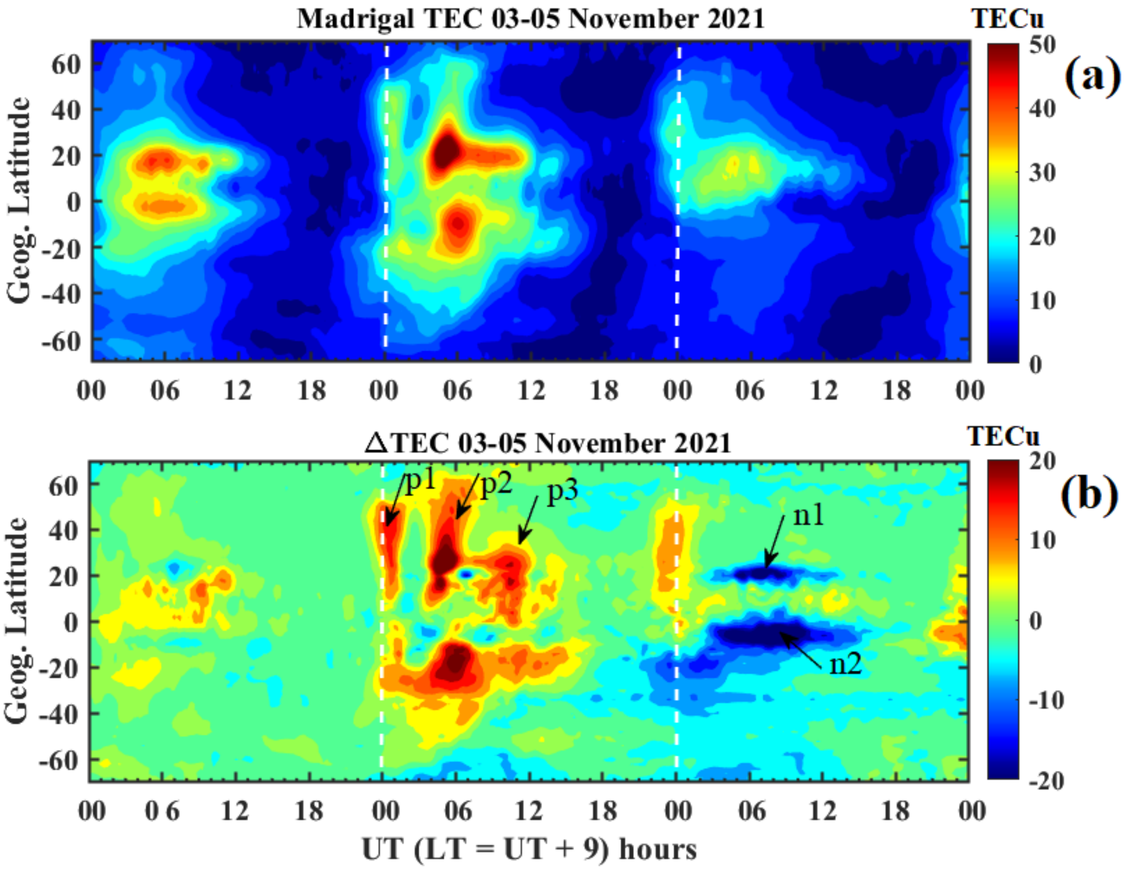
Madrigal TEC 03-05 November 2021
TECu
(a)
Geog. Latitude
UT (LT = UT + 9) hours
ΔTEC 03-05 November 2021
TECu
(b)
p1
p2
p3
n1
n2

**Figure 4 (a-b)**

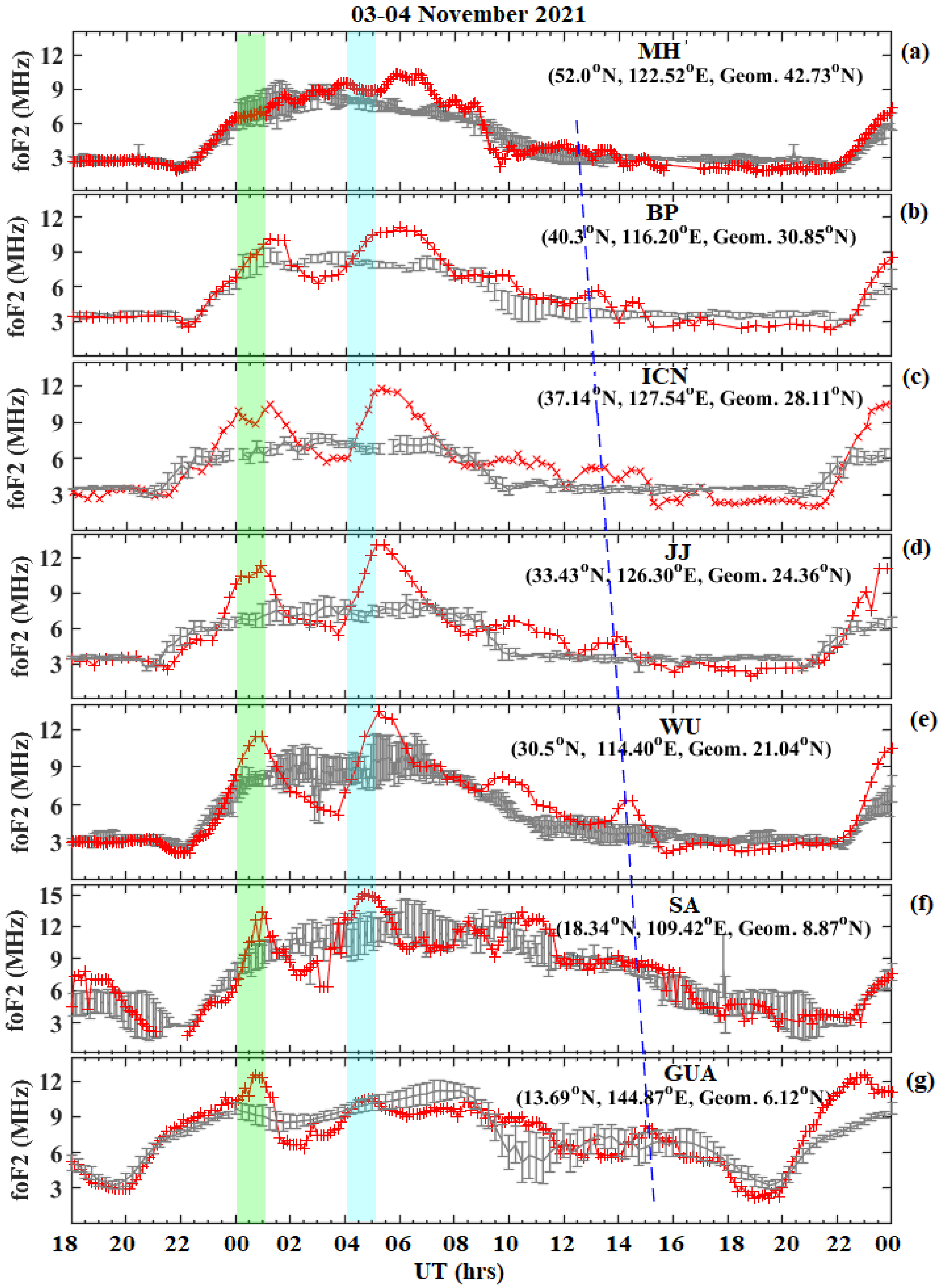


809

810

811 **Figure 5 (a-g)**

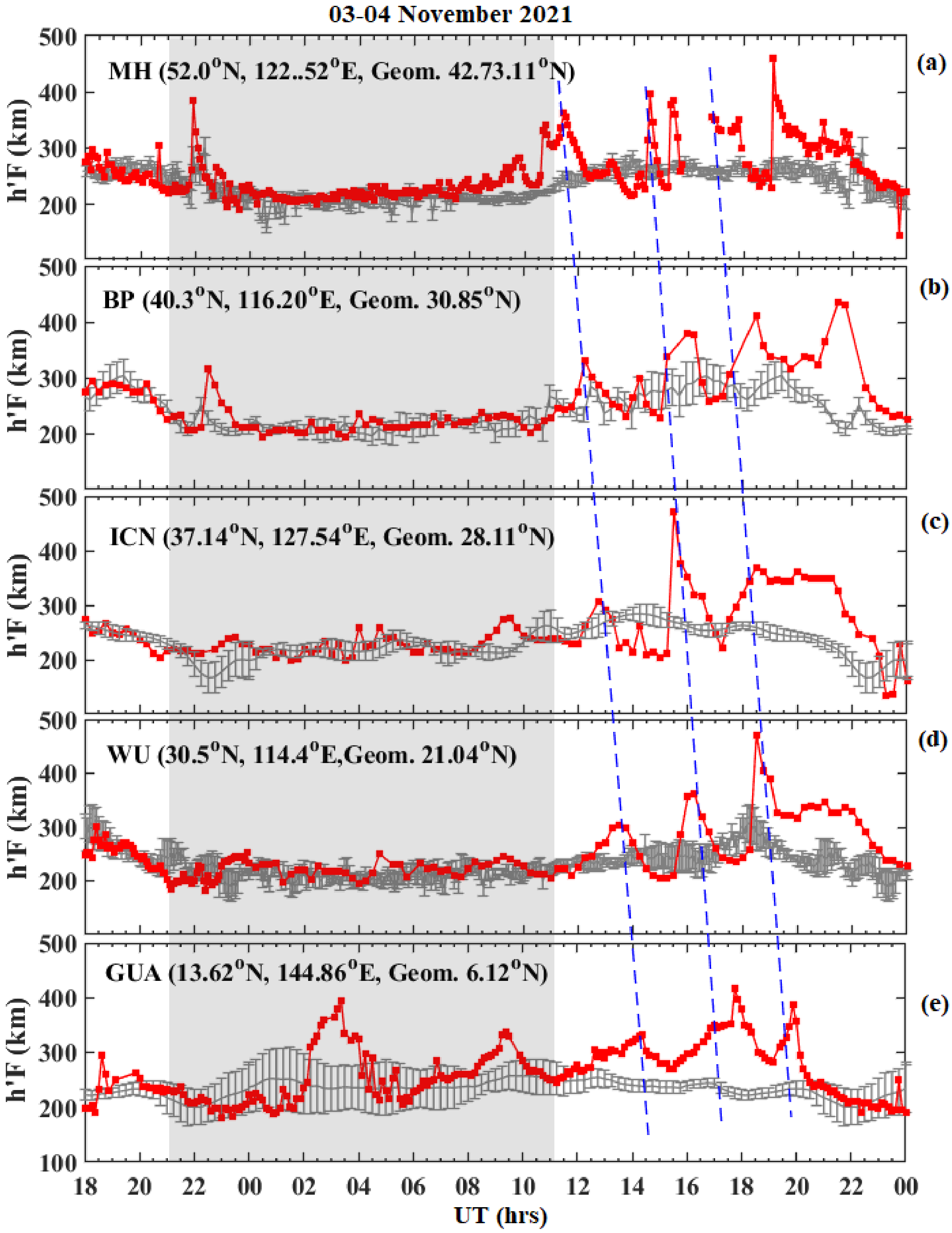
03-04 November 2021
MH (52.0°N, 122..52°E, Geom. 42.73.11°N)
BP (40.3°N, 116.20°E, Geom. 30.85°N)
ICN (37.14°N, 127.54°E, Geom. 28.11°N)
WU (30.5°N, 114.4°E,Geom. 21.04°N)
GUA (13.62°N, 144.86°E, Geom. 6.12°N)
(a)
(b)
(c)
(d)
(e)
h'F (km)
UT (hrs)

Figure 6 (a-e)

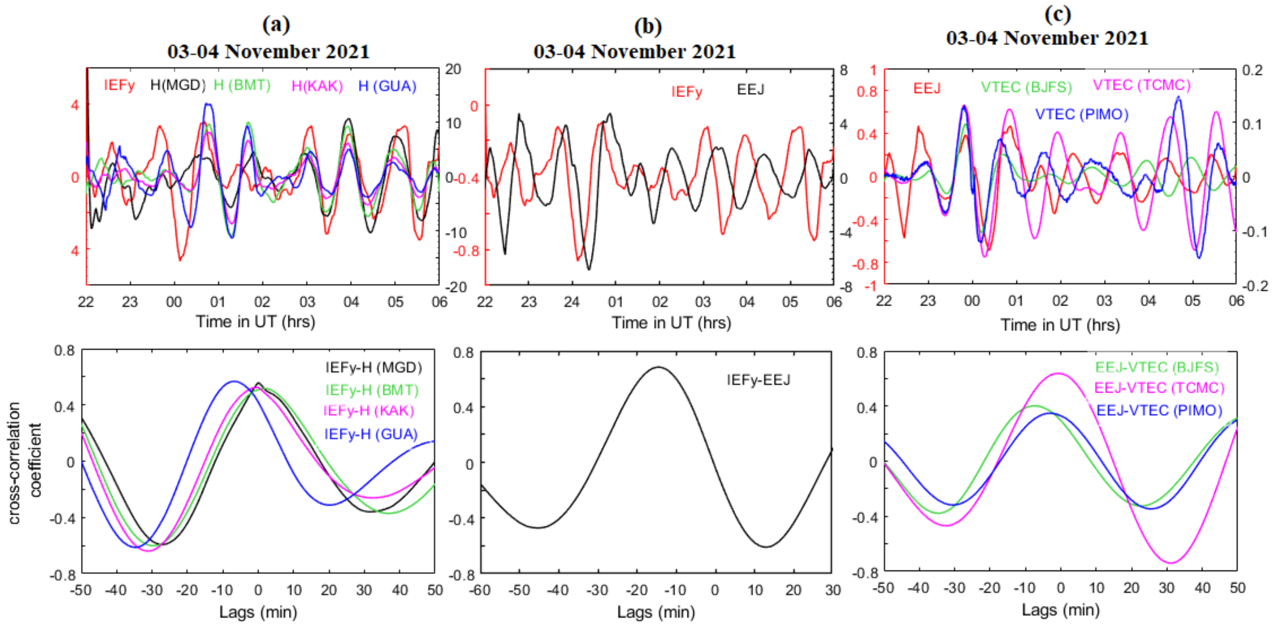
(a)
03-04 November 2021
IEFy
H(MGD)
H (BMT)
H(KAK)
H (GUA)
Time in UT (hrs)
(b)
03-04 November 2021
IEFy
EEJ
Time in UT (hrs)
(c)
03-04 November 2021
EEJ
VTEC (BJFS)
VTEC (TCMC)
VTEC (PIMO)
Time in UT (hrs)
cross-correlation coefficient
IEFy-H (MGD)
IEFy-H (BMT)
IEFy-H (KAK)
IEFy-H (GUA)
Lags (min)
IEFy-EEJ
Lags (min)
EEJ-VTEC (BJFS)
EEJ-VTEC (TCMC)
EEJ-VTEC (PIMO)
Lags (min)

**Figure 7(a-c)**

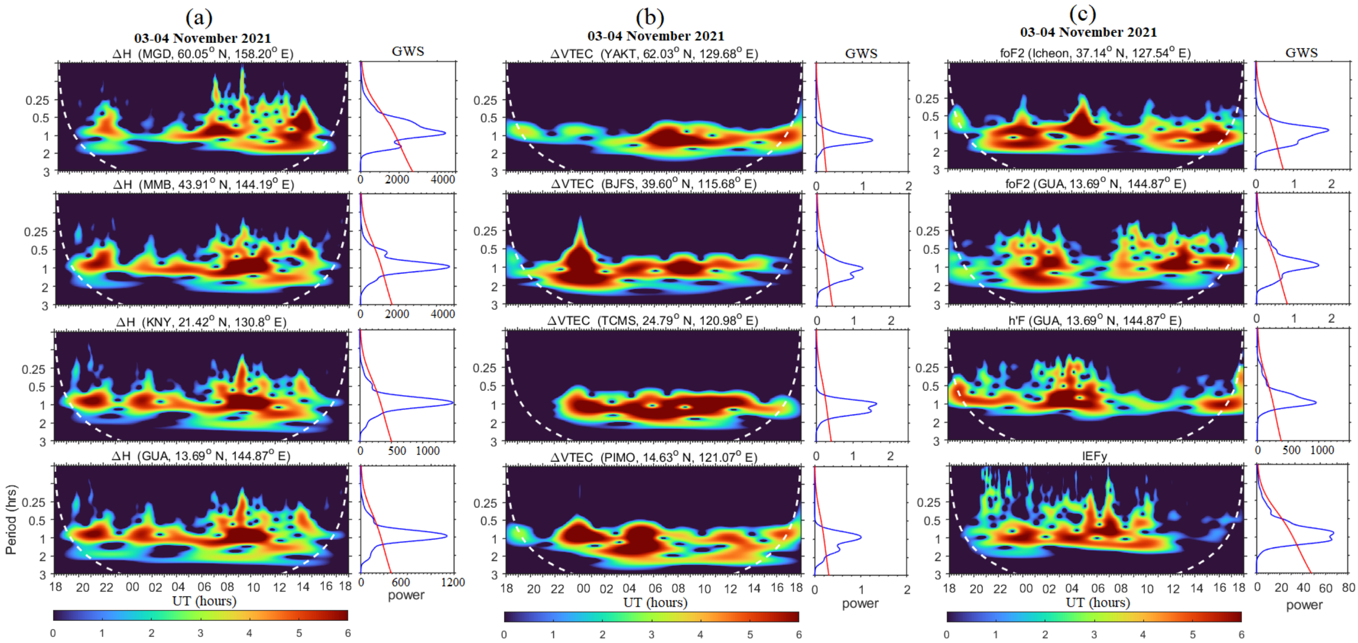
(a)
03-04 November 2021
ΔH (MGD, 60.05° N, 158.20° E)
ΔH (MMB, 43.91° N, 144.19° E)
ΔH (KNY, 21.42° N, 130.8° E)
ΔH (GUA, 13.69° N, 144.87° E)
(b)
03-04 November 2021
ΔVTEC (YAKT, 62.03° N, 129.68° E)
ΔVTEC (BJFS, 39.60° N, 115.68° E)
ΔVTEC (TCMS, 24.79° N, 120.98° E)
ΔVTEC (PIMO, 14.63° N, 121.07° E)
(c)
03-04 November 2021
foF2 (Icheon, 37.14° N, 127.54° E)
foF2 (GUA, 13.69° N, 144.87° E)
h'F (GUA, 13.69° N, 144.87° E)
IEFy
GWS
Period (hrs)
UT (hours)
power

**Figure 8(a-c)**